Journal of Physics B: Atomic, Molecular and Optical Physics

PAPER

Dielectronic recombination in O^{4+} near the ionization threshold

To cite this article: M S Pindzola *et al* 2021 *J. Phys. B: At. Mol. Opt. Phys.* **54** 115205

View the article online for updates and enhancements.

You may also like

- Ion chemistry in space
M Larsson, W D Geppert and G Nyman
- Low-frequency Carbon Radio Recombination Lines. I. Calculations of Departure Coefficients
F. Salgado, L. K. Morabito, J. B. R. Oonk et al.
- The dielectronic recombination of Ar^{+}–Ar^{4+}
I Arnold, E Thomas, S D Loch et al.

IOP ebooks™

Bringing together innovative digital publishing with leading authors from the global scientific community.

Start exploring the collection–download the first chapter of every title for free.

This content was downloaded from IP address 131.204.254.113 on 03/04/2022 at 22:40

IOP Publishing Journal of Physics B: Atomic, Molecular and Optical Physics
J. Phys. B: At. Mol. Opt. Phys. **54** (2021) 115205 (6pp) https://doi.org/10.1088/1361-6455/abc7fe

Dielectronic recombination in O^{4+} near the ionization threshold

M S Pindzola*, M R Fogle and S D Loch

Department of Physics, Auburn University, Auburn, AL, United States

E-mail: pindzola@physics.auburn.edu

Received 12 June 2020, revised 16 October 2020
Accepted for publication 5 November 2020
Published 8 June 2021

Abstract

Relativistic perturbation theory calculations are carried out for dielectronic recombination cross sections involving *jj* J levels near the ionization threshold. We included levels in the $1s^22p^23l$, $1s^22s2p3l$, $1s^22s2p4l$, $1s^22s2p5l$, and $1s^22s2p6l$ configurations of O^{3+} that lie within ± 5.0 eV of the O^{4+} ionization threshold. Theoretical dielectronic recombination cross sections are compared with experimental dielectronic recombination rate coefficients from 0.0 eV to 5.0 eV above threshold.

Keywords: dielectronic, recombination, ionization

(Some figures may appear in colour only in the online journal)

1. Introduction

Resonance states near the ionization threshold may contribute to dielectronic recombination in astrophysical and laboratory plasmas [1, 2]. Proper inclusion of the below-threshold resonance states may make substantial changes in the thermally averaged rate coefficients. Recently below-threshold recombination was discovered in various astrophysical environments. For dielectronic recombination in $C^{2+}1s^22s^2$ below threshold recombination resonances associated with three lines in the $C^+1s^22s2p3d$ configuration were predicted and observed [3]. For dielectronic recombination in $C^{3+}1s^22s$ a below threshold recombination resonance associated with a line in the $C^{2+}1s^22p4p$ configuration was also predicted and observed [3].

For above threshold dielectronic recombination in oxygen atomic ions, theoretical calculations were made thirty years ago using a configuration-average distorted-wave method that included the effects of external fields [4]. Fifteen years later dielectronic recombination in C^{2+}, N^{3+}, and O^{4+} leading to above threshold resonances was studied extensively [5]. Theoretical resonances were determined using the multiconfiguration distorted-wave AUTOSTRUCTURE code of [6, 7], while experimental resonances were obtained using the synchrotron storage ring CRYRING [8]. For dielectronic recombination in $O^{4+}1s^22s^2$, theory and experiment were compared for all the above threshold resonances ranging from threshold to 20 eV. Since that time the CRYRING has been moved from the Manne Siegbahn Laboratory in Stockholm, Sweden to the FAIR complex in Darmstadt, Germany [9]. New experimental measurements will be made for dielectronic recombination in Oxygen atomic ions, with a possible extension to resonances just below threshold.

In this paper we extend our studies of dielectronic recombination to include resonance states above and below threshold for $O^{4+}1s^22s^2$. We only consider those resonances that lie between -5.0 eV and 5.0 eV. The $O^{3+}1s^22p^23l(l = 0, 1, 2)$ configurations contributed 57 levels, the $O^{3+}1s^22s2p3l(l = 2)$ configuration only 6 levels, the $O^{3+}1s^22s2p4l(l = 0, 1, 2)$ configurations contributed 48 levels, the $O^{3+}1s^22s2p5l(l = 0, 1, 2)$ configurations 48 levels, and the $O^{3+}1s^22s2p6l(l = 0, 1, 2)$ configurations 48 levels. We present theoretical dielectronic recombination cross sections for the 207 levels from -5.0 eV below threshold to 5.0 eV above threshold. We compare theoretical dielectronic recombination cross sections with experimental dielectronic recombination rate coefficients [8] from 0.0 eV to 5.0 eV above threshold.

The rest of the paper is structured as follows: in section 2 we review theory, in section 3 we present results, and in section we give a brief summary. Unless otherwise stated, all quantities are given in atomic units.

* Author to whom any correspondence should be addressed.

 © 2021 IOP Publishing Ltd Printed in the UK

2. Theory

The dielectronic recombination cross section for an N electron ground level with statistical weight g_i combining into an $(N+1)$ electron doubly excited level with statistical weight g_j is given by [10]

$$\sigma_{i\to j} = \frac{\pi^2}{E_c \Delta E_c} \frac{g_j}{2g_i} A_a(j \to i) B_j \tag{1}$$

where E_c is the energy of the continuum electron and ΔE_c is bin width. The branching ratio for radiative stabilization is given by

$$B_j = \frac{\sum_n A_r(j \to n)}{\sum_k A_a(j \to k) + \sum_n A_r(j \to n)}, \tag{2}$$

where the radiative rate is given by

$$A_r(j \to n) = 2\pi | < n|D|j > |^2, \tag{3}$$

where D is the dipole radiation field operator, and the autoionization rate is given by

$$A_a(j \to n) = 4/k | < n|V|j > |^2, \tag{4}$$

where V is the electrostatic interaction between electrons. The electron linear momentum is taken as $k = \sqrt{2|E_{jn}|}$ for the evaluation of the autoionization rates.

A multi-configuration fully-relativistic atomic structure code [11] is used to calculate the bound state wavefunctions. The radial Dirac equation with a local exchange potential is used to calculate the continuum radial orbitals. Convoluted cross sections are obtained using a Gaussian energy distribution.

3. Results

3.1. Target ion energies

Fully relativistic calculations were carried out for the $O^{4+}1s^22s^2$ configuration leading to an energy of -68.3032 a.u. Fully relativistic calculations were also carried out for the O^{4+} $(1s^22s^2 + 1s^22p^2)$ configurations leading to an energy of -68.3970 a.u. Energies are based on differences between low-order relativistic calculations for the resonance configurations and fully-relativistic calculations for the O^{4+} $(1s^22s^2 + 1s^22p^2)$ configuration.

3.2. $1s^22p^23l$ configurations

Low-order relativistic calculations were carried out for the 8 levels of the even-parity $O^{3+}1s^22p^23s$ configuration. For added correlation we also included 9 levels from the $1s^22s^22p^2$ and $1s^22s^23s$ configurations. Autoionization rates were determined for the decay of the 8 levels of the $1s^22p^23s$ configuration to the 30 levels of the $1s^22s2pkp$ and $1s^22s2pkf$ configurations. Radiative rates were determined for the decay of the 8 levels of the $1s^22p^23s$ configuration to the 5 levels of the $1s^22p^3$ configuration. Dielectronic recombination cross sections for the 8 levels are presented in figure 1 (upper) using $\Delta E_c = 0.04$ eV in equation (1). Convoluted dielectronic recombination cross sections for the 8 levels are presented in figure 2 (upper) using a convolution energy of 0.4 eV. We note that the largest convoluted cross section is around -2.0 eV due to the levels $1s^22p^2(0)3s1/2$ and $1s^22p^2(2)3s3/2$, where the allowed states for jj coupling of $2p^2$ are (0) and (2).

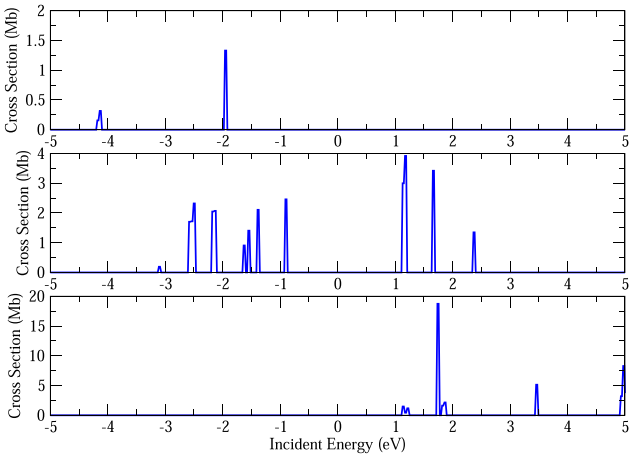

Figure 1. Dielectronic recombination cross sections. Upper row: $1s^22p^23s$, middle row: $1s^22p^23p$, lower row: $1s^22p^23d$. (1.0 Mb $= 1.0 \times 10^{-18}$ cm^2).

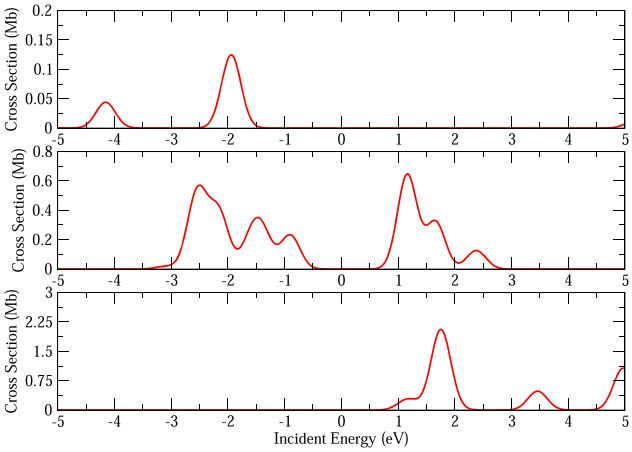

Figure 2. Convoluted Dielectronic recombination cross sections. Upper row: $1s^22p^23s$, middle row: $1s^22p^23p$, lower row: $1s^22p^23d$. (1.0 Mb $= 1.0 \times 10^{-18}$ cm^2).

Low-order relativistic calculations were carried out for the 21 levels of the odd-parity $O^{3+}1s^22p^23p$ configuration. For added correlation we also included 4 levels from the $1s^22s^22p$ and $1s^22s^23p$ configurations. Autoionization rates were determined for the decay of the 21 levels of the $1s^22p^23p$ configuration to the 41 levels of the $1s^22s2pks$, $1s^22s2pkd$, and $1s^22s2pkg$ configurations. Radiative rates were determined for the decay of the 21 levels of the $1s^22p^23p$ configuration to the 8 levels of the $1s^22s2p^2$ configuration. Dielectronic recombination cross sections for the 21 levels are presented in figure 1 (middle) using $\Delta E_c = 0.04$ eV in equation (1). Convoluted dielectronic recombination cross sections for the 21 levels are presented in figure 2 (middle) using a convolution

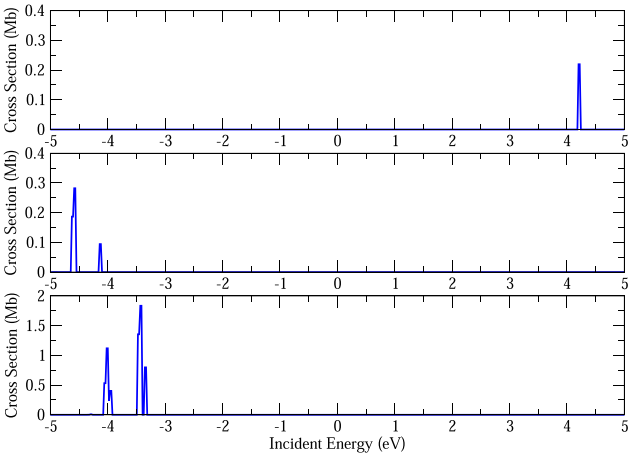

Figure 3. Dielectronic recombination cross sections. Upper row: $1s^22s2p4s$, middle row: $1s^22s2p4p$, lower row: $1s^22s2p4d$. (1.0 Mb = 1.0 × 10 $^{-18}$ cm^2).

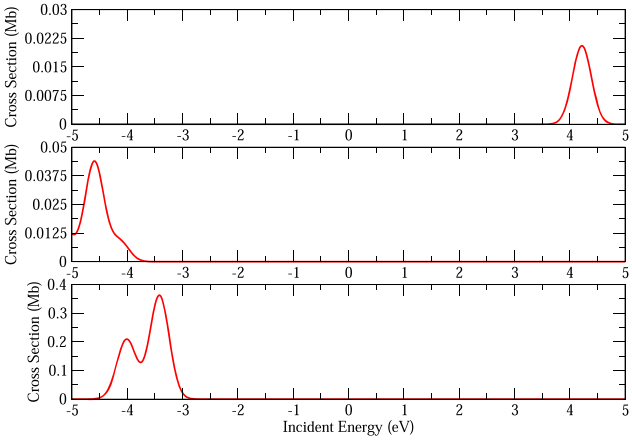

Figure 4. Convoluted Dielectronic recombination cross sections. Upper row: $1s^22s2p4s$, middle row: $1s^22s2p4p$, lower row: $1s^22s2p4d$. (1.0 Mb = 1.0 × 10 $^{-18}$ cm^2).

energy of 0.4 eV. We note that the largest convoluted cross section is around 1.2 eV due to the levels $1s^22p^2(2)3p3/2$ and $1s^22p^2(2)3p5/2$.

Low-order relativistic calculations were carried out for the 28 levels of the even-parity $O^{3+}1s^22p^23d$ configuration. For added correlation we also included 10 levels from the $1s^22s2p^2$ and $1s^22s^23d$ configurations. Autoionization rates were determined for the decay of the 28 levels of the $1s^22p^23d$ configuration to the 53 levels of the $1s^22s2pkp$, $1s^22s2pkf$, and $1s^22s2pkh$ configurations. Radiative rates were determined for the decay of the 28 levels of the $1s^22p^23d$ configuration to the 5 levels of the $1s^22p^3$ configuration. Dielectronic recombination cross sections for the 28 levels are presented in figure 1 (lower) using $\Delta E_c = 0.04$ eV in equation (1). Convoluted dielectronic recombination cross sections for the 28 levels are presented in figure 2 (lower) using a convolution energy of 0.4 eV. We note that the largest convoluted cross section is around 1.7 eV due to the levels $1s^22p^2(2)3d3/2$, $1s^22p^2(2)3d5/2$, and $1s^22p^2(2)3d7/2$.

3.3. $1s^22p^24l$ configurations

Low-order relativistic calculations for the $O^{3+}1s^22p^24l$ ($l = 0$–3) configurations were found to have level energies of 10.0 eV and above and were not considered.

3.4. $1s^22s2p3l$ configurations

Low-order relativistic calculations were carried out for the 7 levels of the $O^{3+}1s^22s2p3s$ configuration, the 18 levels of the $O^{3+}1s^22s2p3p$ configuration, and the 23 levels of the $O^{3+}1s^22s2p3d$ configuration. Only 6 levels of the $1s^22s2p3d$ subconfiguration were found to have level energies above −5.00 eV.

3.5. $1s^22s2p4l$ configurations

Low-order relativistic calculations were carried out for the 7 levels of the odd-parity $O^{3+}1s^22s2p4s$ configuration. For added correlation we also included 2 levels from the $1s^22s^22p$ configuration. Autoionization rates were determined for the decay of the 7 levels of the $1s^22s2p4s$ configuration to the 3 levels of the $1s^22s^2kp$ and $1s^22s^2kf$ configurations. Radiative rates were determined for the decay of the 7 levels of the $1s^22s2p4s$ configuration to the 8 levels of the $1s^22s2p^2$ configuration. Dielectronic recombination cross sections for the 7 levels are presented in figure 3 (upper) using $\Delta E_c = 0.04$ eV in equation (1). Convoluted dielectronic recombination cross sections for the 7 levels are presented in figure 4 (upper) using a convolution energy of 0.4 eV. We note that the largest convoluted cross section is around 4.2 eV due to the levels $1s^22s2p(2)4s3/2$ and $1s^22s2p(2)4s5/2$.

Low-order relativistic calculations were carried out for the 18 levels of the even-parity $O^{3+}1s^22s2p4p$ configuration. For added correlation we also included 8 levels from the $1s^22s2p^2$ configuration. Autoionization rates were determined for the decay of the 18 levels of the $1s^22s2p4p$ configuration to the 4 levels of the $1s^22s^2ks$, $1s^22s^2kd$, and $1s^22s^2kg$ configurations. Radiative rates were determined for the decay of the 18 levels of the $1s^22s2p4p$ configuration to the 2 levels of the $1s^22s^22p$ configuration. Dielectronic recombination cross sections for the 18 levels are presented in figure 3 (middle) using $\Delta E_c = 0.04$ eV in equation (1). Convoluted dielectronic recombination cross sections for the 18 levels are presented in figure 4 (middle) using a convolution energy of 0.4 eV. We note that the largest convoluted cross section is around −4.5 eV due to the level $1s^22s2p(1)4p1/2$.

Low-order relativistic calculations were carried out for the 23 levels of the odd-parity $O^{3+}1s^22s2p4d$ configuration. For added correlation we also included 2 levels from the $1s^22s^22p$ configuration. Autoionization rates were determined for the decay of the 23 levels of the $1s^22s2p4d$ configuration to the 5 levels of the $1s^22s^2kp$, $1s^22s^2kf$, and $1s^22s^2kh$ configurations. Radiative rates were determined for the decay of the 23 levels of the $1s^22s2p4d$ configuration to the 8 levels of the $1s^22s2p^2$ configuration. Dielectronic recombination cross sections for the 23 levels are presented in figure 3 (lower) using $\Delta E_c = 0.04$ eV in equation (1). Convoluted dielectronic recombination cross sections for the 23 levels are presented in

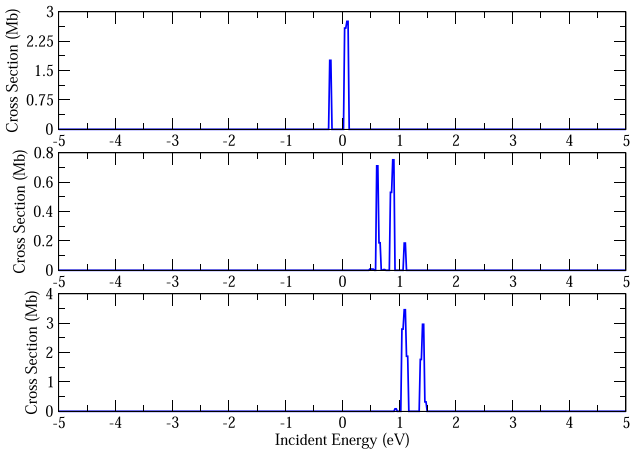

Figure 5. Dielectronic recombination cross sections. Upper row: $1s^22s2p5s$, middle row: $1s^22s2p5p$, lower row: $1s^22s2p5d$. (1.0 Mb = 1.0 × 10 $^{-18}$ cm^2).

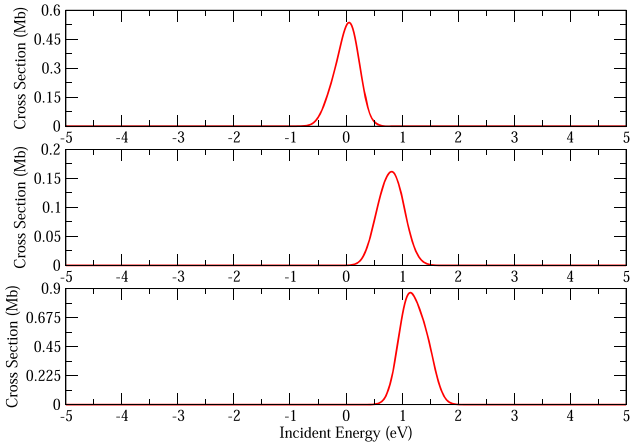

Figure 6. Convoluted Dielectronic recombination cross sections. Upper row: $1s^22s2p5s$, middle row: $1s^22s2p5p$, lower row: $1s^22s2p5d$. (1.0 Mb = 1.0 × 10 $^{-18}$ cm^2).

figure 4 (lower) using a convolution energy of 0.4 eV. We note that the largest convoluted cross sections is around −3.5 eV due to the level $1s^22s2p(1)4d7/2$.

Low-order relativistic calculations for the 24 levels of the $O^{3+}1s^22s2p4f$ configuration were found to have small dielectronic recombination cross sections.

3.6. 1s2s2p5l configurations

Low-order relativistic calculations were carried out for the 7 levels of the $O^{3+}1s^22s2p5s$ configuration, the 18 levels of the $O^{3+}1s^22s2p5p$ configuration, the 23 levels of the $O^{3+}1s^22s2p5d$ configuration, the 24 levels of the $O^{3+}1s^22s2p5f$ configuration, and the 24 levels of the $O^{3+}1s^22s2p5g$ configuration. Dielectronic recombination cross sections for the 48 levels of the $O^{3+}1s^22s2p5l$ ($l = 0, 1, 2$) configurations are presented in figure 5 using $\Delta E_c = 0.04$ eV in equation (1). Convoluted dielectronic recombination cross sections for the 48 levels are presented in figure 6 using a convolution energy of 0.4 eV.

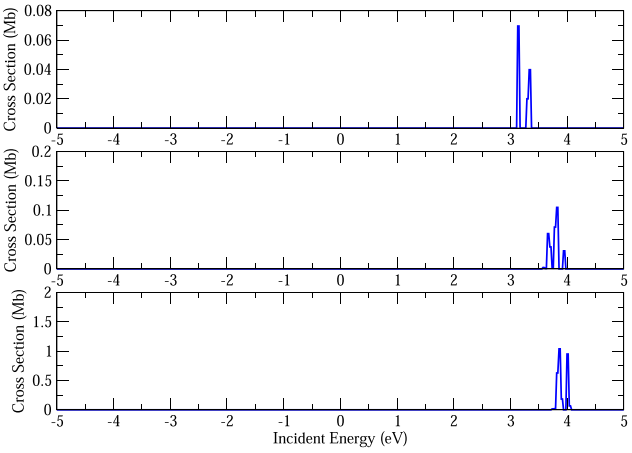

Figure 7. Dielectronic recombination cross sections. Upper row: $1s^22s2p6s$, middle row: $1s^22s2p6p$, lower row: $1s^22s2p6d$. (1.0 Mb = 1.0 × 10 $^{-18}$ cm^2).

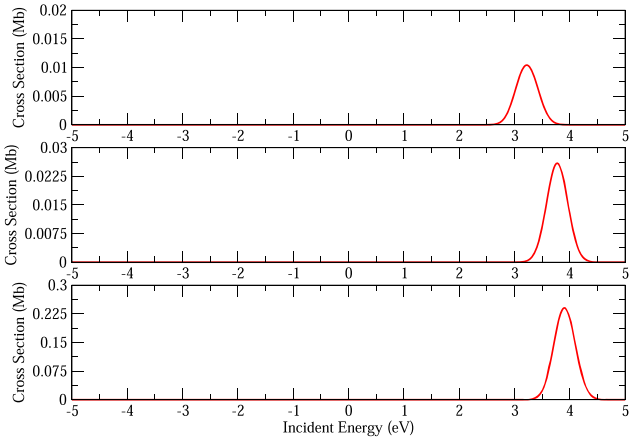

Figure 8. Convoluted Dielectronic recombination cross sections. Upper row: $1s^22s2p6s$, middle row: $1s^22s2p6p$, lower row: $1s^22s2p6d$. (1.0 Mb = 1.0 × 10 $^{-18}$ cm^2).

Low-order relativistic calculations for the 24 levels of the $O^{3+}1s^22s2p5f$ configuration and the 24 levels of the $O^{3+}1s^22s2p5g$ configuration were found to have small dielectronic recombination cross sections.

3.7. 1s2s2p6l configurations

Low-order relativistic calculations were carried out for the 7 levels of the $O^{3+}1s^22s2p6s$ configuration, the 18 levels of the $O^{3+}1s^22s2p6p$ configuration, and the 23 levels of the $O^{3+}1s^22s2p6d$ configuration. Dielectronic recombination cross sections for the 48 levels of the $O^{3+}1s^22s2p6l$ ($l = 0, 1, 2$) configurations are presented in figure 7 using $\Delta E_c = 0.04$ eV in equation (1). Convoluted dielectronic recombination cross sections for the 48 levels are presented in figure 8 using a convolution energy of 0.4 eV.

Low-order relativistic calculations for each of the 24 levels of the $O^{3+}1s^22s2p6l(l = 3–5)$ configurations were assumed to have small dielectronic recombination cross sections.

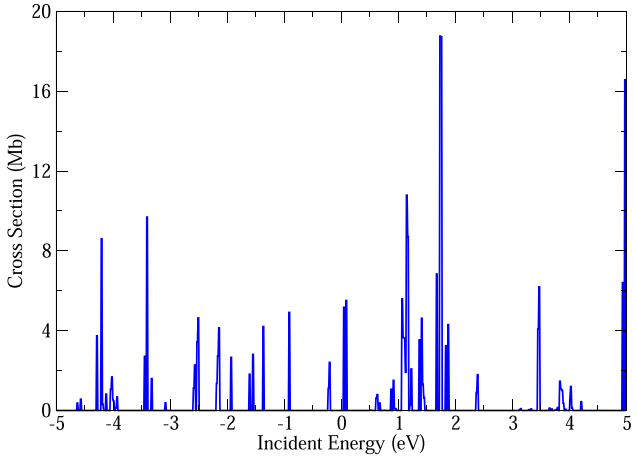

Figure 9. Total dielectronic recombination cross sections (1.0 Mb = 1.0 × 10 $^{-18}$ cm^2).

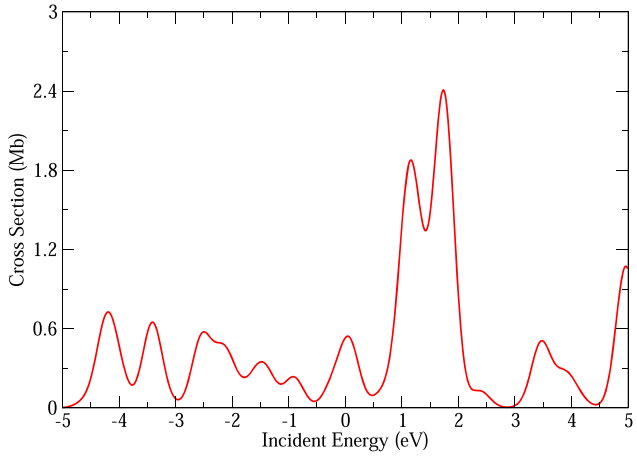

Figure 10. Total convoluted dielectronic recombination cross sections (1.0 Mb = 1.0 × 10 $^{-18}$ cm^2).

3.8. 1s2s2p7l configurations

Low-order relativistic calculations were carried out for the 7 levels of the $O^{3+}1s^22s2p7s$ configuration and all were found to have energies above 5.00 eV and were not considered.

3.9. Total cross sections

Total dielectronic recombination cross sections combining cross sections for the $1s^22p^23l(l = 0, 1, 2)$, $1s^22s2p3d$, $1s^22s2p4l(l = 0, 1, 2)$, $1s^22s2p5l(l = 0, 1, 2)$, and $1s^22s2p6l(l = 0, 1, 2)$ configurations are presented in figure 9 using $\Delta E_c = 0.04$ eV in equation (1). Total convoluted dielectronic recombination cross sections for all the configurations are presented in figure 10 using a convolution energy of 0.4 eV. The largest convoluted cross section is between 1.0 eV and 2.0 eV.

3.10. Comparison with experiment

Theoretical dielectronic recombination cross sections using $\Delta E_c = 0.04$ eV are compared with theoretical and experimental dielectronic recombination rate coefficients [5] from 0.0 eV to 5.0 eV above threshold Figure 11. Current theory, previous theory [5], and experiment [5] find a number of

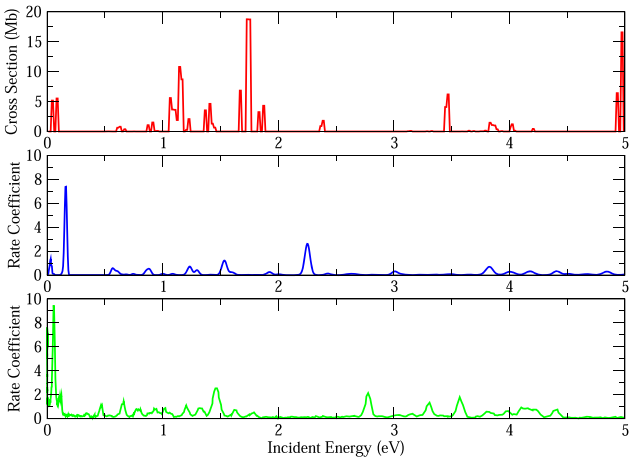

Figure 11. Upper graph: theoretical dielectronic recombination cross sections ($\Delta E_c = 0.04$ eV). Middle graph: theoretical dielectronic recombination rate coefficients [5]. Lower graph: experimental dielectronic recombination rate coefficients [5]. (1.0 Mb = 1.0 × 10 $^{-18}$ cm^2)

strong resonances between 0.0 eV and 3.0 eV above threshold. Current theory, previous theory [5], and experiment [5] also find a smaller number of weaker resonances between 3.0 eV and 5.0 eV above threshold. The set of current theory resonances at 5.0 eV are slightly below previous theoretical [5] and experimental [5] resonances found just above 5.0 eV.

Considering the differences between the theoretical and the experimental results, the low energy resonances in the experimental measurements are in general in good agreement with level energies given in the NIST database. Thus the fact that the theoretical results are different from experiment demonstrates that further work is required on the theoretical side to produce accurate low temperature dielectronic recombination rate coefficients for this system. This is also reflected in the fact that resonance positions in the theory calculations are sensitive to the size of the configuration-interaction expansion in the calculations. Dielectronic recombination calculations for O are particularly challenging due to the presence of triply excited states in the low energy region. Thus the current low temperature dielectronic recombination rate coefficients in databases for O^{4+} likely have sizable uncertainties and further theoretical investigation is required.

4. Summary

Relativistic perturbation theory has been applied to calculate the dielectronic recombination in O^{4+} above and below the ionization threshold involving levels in the $O^{3+}1s^22p^23l$, $O^{3+}1s^22s2p3l$, $O^{3+}1s^22s2p4l$, $O^{3+}1s^22s2p5l$, and $O^{3+}1s^22s2p6l$ configurations. Theoretical dielectronic recombination cross sections were compared to experimental dielectronic recombination rate coefficients [5] from 0.0 eV to 5.0 eV above threshold.

In the future we plan to make more dielectronic recombination cross section calculations that include below threshold resonances. Efforts are also being made to extend the experimental cross section measurements to below threshold, but it will be very difficult.

Acknowledgments

This work was supported in part by grants from the US National Aeronautics and Space Administration and the US Department of Energy. Computational work was carried out at the National Energy Research Scientific Computing Center (NERSC) in Berkeley, California.

ORCID iDs

M S Pindzola https://orcid.org/0000-0001-6787-9249

References

[1] Robicheaux F, Loch S D, Pindzola M S and Ballance C P 2010 *Phys. Rev. Lett.* **105** 233201

[2] Pindzola M S, Loch S D and Robicheaux F 2011 *Phys. Rev.* A **83** 042705

[3] Nemer A, Sterling N C, Raymond J, Dupree A K, García-Rojas J, Wang Q, Pindzola M S, Ballance C P and Loch S D 2019 *Astrophys. J.* **887** L9

[4] Krylstedt P, Pindzola M S and Badnell N R 1990 *Phys. Rev.* A **41** 2506

[5] Fogle M, Badnell N R, Glans P, Loch S D, Madzunkov S, Abdel-Naby S A, Pindzola M S and Schuch R 2005 *Astron. Astrophys.* **442** 757

[6] Badnell N R 1986 *J. Phys. B: At. Mol. Phys.* **19** 3827

[7] Badnell N R 2001 *ASP Conf. Ser.* **247** 37

[8] Electron beam ion source (CRYSIS) and Storage RING.

[9] Lestinsky M A *et al* 2015 *Phys. Scr.* **T166** 014075

[10] Bräuning-Demian M S and Badnell N R 1990 *Phys. Rev.* A **42** 6526

[11] Grant I P 2007 *Relativistic Quantum Theory of Atoms and Molecules* (New York: Springer)